

## Microwave-induced thermoacoustic imaging with functional nanoparticles

Xiaoyu Tang<sup>\*,†</sup>, Jia Fu<sup>\*,†</sup> and Huan Qin<sup>\*,†,‡,§</sup>

*\*MOE Key Laboratory of Laser Life Science & Institute of Laser Life Science  
College of Biophotonics, South China Normal University  
Guangzhou 510631, P. R. China*

*†Guangdong Provincial Key Laboratory of Laser Life Science,  
College of Biophotonics, South China Normal University,  
Guangzhou 510631, P. R. China*

*‡Guangzhou Key Lab of Spectral Analysis and Functional Probes,  
College of Biophotonics  
South China Normal University, Guangzhou 510631, P. R. China  
§qinghuan@scnu.edu.cn*

Received 24 July 2022

Revised 30 August 2022

Accepted 18 September 2022

Published 9 November 2022

As an emerging hybrid imaging modality, microwave-induced thermoacoustic imaging (MTAI), using microwaves as the excitation source and ultrasonic signals as the information carrier for combining the characteristics of high contrast of electromagnetic imaging and high resolution of ultrasound imaging, has shown broad prospects in biomedical and clinical applications. The imaging contrast depends on the microwave-absorption coefficient of the endogenous imaged tissue and the injected MTAI contrast agents. With systemically introduced functional nanoparticles, MTAI contrast and sensitivity can be further improved, and enables visualization of biological processes *in vivo*. In recent years, functional nanoparticles for MTAI have been developed to improve the performance and application range of MTAI in biomedical applications. This paper reviews the recent progress of functional nanoparticles for MTAI and their biomedical applications. The challenges and future directions of microwave thermoacoustic imaging with functional nanoparticles in the field of translational medicine are discussed.

**Keywords:** Microwave thermoacoustic imaging; nanomaterials; nanoprobe.

### 1. Introduction

Medical imaging is an essential diagnostic technique in clinical diagnosis of diseases. Among the existing

medical imaging techniques, nuclear magnetic resonance (NMR) imaging based on a biomagnetic spin imaging technique, which has been widely used

<sup>§</sup>Corresponding author.

for clinical imaging, with high-sensitivity, but expensive, long detection time and not convenient for tumor screening to some extent.<sup>1–5</sup> X-ray imaging uses the difference in absorption of X-rays by biological tissues to achieve imaging of *in vivo* structures and detection of tumors, but X-rays have radiation hazards for related people.<sup>6–11</sup> Ultrasound (US) imaging is based on the difference in acoustic impedance between biological tissues to form different ultrasound echo signals for the purpose of disease detection. When the diseased tissue is small or the difference in acoustic impedance with the surrounding normal tissue is small, the image has poor contrast, which is difficult to achieve high-sensitivity tumor detection.<sup>12–19</sup> Optical imaging techniques have the characteristics of high-resolution and high contrast in tumor imaging. They are difficult to achieve high-resolution imaging in deep tissues as the resolution gradually decreases with depth due to light scattering effect.<sup>20–27</sup> Therefore, an imaging technology with high-sensitivity, high-resolution, high contrast, low cost and few side effects that can achieve deep tissue imaging has become a hot research topic in the field of medical imaging.

The thermoacoustic (TA) effect was first discovered in 1880 by Bell.<sup>28</sup> In the 1980s, Professor Bowen<sup>29</sup> was the first to apply it to soft tissue imaging. Microwave thermoacoustic imaging (MTAI) is the absorption of energy by biological tissues under short pulse microwave conditions, resulting in a small instantaneous temperature rise, leading to thermal expansion effects, and excitation of the ultrasonic range of thermoacoustic signals.<sup>30</sup> Its thermoacoustic signal carries the information of microwave-absorption characteristics of the tissue. By collecting the thermoacoustic signal around the tissue, image inversion is applied to reconstruct the structure and morphology of biological tissue into other information, as shown in Fig. 1. In the frequency range of 0.1 to 10 GHz, the relative permittivity of soft tissues is 5 to 70 and the conductivity is 0.02 to 3 S/m. The dielectric properties of biological tissues determine their absorption of microwaves at different frequency conditions. Therefore, the dielectric properties of biological tissues at different locations can be deduced from MTAI to obtain the corresponding tissue structure and location information.<sup>31–34</sup> Different from photoacoustic imaging (PAI), MTAI uses microwaves as the excitation source, and

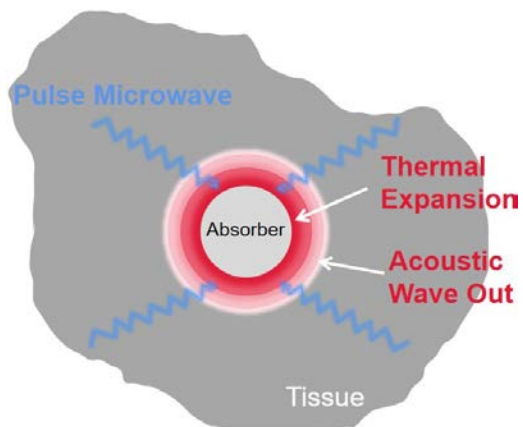


Fig. 1. Schematic diagram of thermoacoustic effect.

microwaves can achieve about 15 cm imaging depth, as well as high-resolution imaging at centimeter depth,<sup>30</sup> showing powerful potential for early lesion tissue detection and tumor detection.

The contrast of MTAI depends mainly on polar molecules (e.g., water, amino acids, glucose) within biological tissues, as well as on the differences in the distribution of ionic concentrations.<sup>35</sup> For example, the microwave absorption of early breast lesioned tissues is 2–10 times higher than normal tissues,<sup>36–38</sup> which is mainly due to the fact that abnormal tissues have higher water and ionic content than normal tissues. Currently, MTAI has been extensively studied in breast tumor detection, brain tissue imaging, joint imaging, prostate tumor imaging, pancreatic tumor imaging, vascular imaging, liver imaging and related disease treatment.<sup>30</sup>

In MTAI, besides imaging with endogenous contrast agents from biological tissues, exogenous functional nanoparticles can also be introduced to auxiliary imaging to detect biological processes *in vivo*. Nanomaterials with excellent microwave-absorption properties, have the potential to improve the performance and application range of MTAI in biomedical applications. The main mechanisms that have been reported for the generation of TA signals by MTAI contrast agents are mainly divided into dielectric loss and magnetic loss, the dielectric loss including polarization loss and conductivity loss.<sup>31</sup> Polarization loss refers to the electric dipoles in the alternating electric field orientation rotating to absorb microwave energy and then generating thermoacoustic signals, due to the existence of vacancy defects in nanomaterials, as the distribution of electron clouds around the vacancy is inhomogeneous, which generates electric dipoles.<sup>39</sup> The

dielectric loss mainly depends on the dielectric whether it contains free ions, which can generate conductive current in the external electric field, so that the partial current consumption will be expressed as thermal energy, then generate the thermoacoustic signal through the thermal expansion effect.<sup>39</sup> Currently, TA functional nanoparticles developed by using dielectric loss mechanism mainly include polyarginine nanomaterials, defective graphene oxide (GO),<sup>40</sup> defect-rich titanium nitride (TiN) nanomaterials,<sup>41</sup> iron-doped black phosphorus (BP) nanomaterials<sup>42</sup> and NaCl nanodroplets,<sup>43</sup> etc. The defect-rich TA functional nanoparticles are mainly modified by atomic substitution doping, surface modification, and interstitial doping to achieve artificial control of the degree of defects in the nanomaterials, which makes nanomaterials with a large number of electric dipoles or free ions.<sup>44,45</sup> Magnetic loss refers to the repeated magnetization of magnetic materials such as ferromagnets in the alternating magnetic field, and part of the electromagnetic energy is irreversibly converted to thermal energy during the repeated magnetization process, which results in thermoacoustic signals.<sup>46–48</sup> As has been explored, ferrites, functionalized Fe<sub>3</sub>O<sub>4</sub> and other magnetic nanomaterials achieved microwave-acoustic conversion process through the principle of magnetic loss.<sup>49–53</sup> With the presence of suitable endogenous contrast agents, MTAI not only enables breast cancer imaging, but also joint-related disease imaging, brain imaging, vascular imaging, and endoscopic imaging.<sup>54–60</sup> In the absence of endogenous contrast agents or with limited detection depth, TA signals in deep tumors can be selectively amplified by introducing exogenous functional nanoparticles. When nanomaterials are used as exogenous functional nanoparticles, it is possible to achieve aggregation at the tumor site by active or passive targeting, thus enhancing MTAI contrast and sensitivity, and help MTAI techniques detect physiological processes indirectly *in vivo*. In addition, exogenous targeted functional nanoparticles combined with pulsed microwave excitation that can destroy tumor cells by thermoacoustic shockwave and thus achieve efficient tumor suppression, showing the dual benefits of targeted therapy and enhanced imaging.<sup>61,62</sup>

In medical imaging techniques, contrast agents all serve an important role, not only to significantly improve the contrast, break the imaging depth

limit, and provide more accurate information related to biological tissues as well as to achieve therapeutic purposes. In this paper, we analyze a series of recently published research results about functional nanoparticles of MTAI. The challenges and future trends of microwave thermoacoustic imaging with functional nanoparticles in translational medicine are discussed.

## 2. Exogenous Functional Nanoparticles

With the development of novel imaging technologies, exogenous functional nanoparticles play an essential role in imaging. Exogenous functional nanoparticles introduced by MTAI include inorganic nanomaterials and organic nanomaterials, and the ideal exogenous functional nanoparticles can significantly improve contrast and sensitivity. In terms of clinical translation, the development of exogenous functional nanoparticles is important for translation of MTAI research into clinical applications.

### 2.1. Inorganic nanomaterials

In this section, inorganic nanomaterials as exogenous functional nanoparticles for MTAI are reviewed in detail. Inorganic nanomaterials as exogenous functional nanoparticles for MTAI mainly include metal oxides, metal nitrides, carbon analogues, black phosphorus and transition metal sulfide contrast agents.

#### 2.1.1. Metal oxides and metal nitrides

Metal oxides such as Fe<sub>3</sub>O<sub>4</sub>, yttrium iron garnet (YIG), and Mn<sub>3</sub>O<sub>4</sub> are materials with certain magnetic properties. Magnetic nanomaterials exhibit good microwave absorption due to their strong magnetic field response and dielectric properties. In addition, metal oxides are characterized by good particle size distribution and simple preparation. Some researchers have attached metal oxides<sup>49–53,63–67</sup> with specific targeting probes to achieve active targeting of cell membranes and mitochondria of tumor cells, thus enhancing the imaging capability and improving the therapeutic efficiency of MTAI, as shown in Table 1.

Carbonyl iron<sup>63</sup> is a 2 μm microsphere with strong microwave absorption. Carbonyl iron obtained by sol-gel process has better hydrophilic,

Table 1. Metal oxide contrast agent for microwave thermoacoustic imaging.

Microwave thermoacoustic contrast agent	Excitation source frequency	Size (nm)	Modification application	Application
Carbonyl iron FA-Fe <sub>3</sub> O <sub>4</sub> /polyaniline (PANI)	1.2 GHz <sup>63</sup> 6 GHz <sup>49</sup>	2000 30–50	Folic acid (FA)	MTAI, in tissue phantoms <i>Ex vivo</i> MTAI in human blood and <i>in vivo</i> MTA tomography (MTAT) in mouse tail, <i>in vivo</i> MTAI of tumors
Dextran-coated Fe <sub>3</sub> O <sub>4</sub> nanoparticles	6 GHz <sup>50</sup>	30–50	Dextran	MTAI, in tissue phantoms
Fe <sub>3</sub> O <sub>4</sub> /Au nanoparticles	6 GHz <sup>51</sup>	30–50	FITC-labeled integrin α <sub>v</sub> β <sub>3</sub> mAb	Triple-modality MRI-MTAI-PAI
Fe <sub>3</sub> O <sub>4</sub>	3 GHz <sup>52</sup>	10	Citrate	MTAI, in tissue phantoms
Human serum albumin (HSA)-functionalized superparamagnetic iron oxide nanoparticles (HSA-SPIO)	434 MHz <sup>53</sup>	210–260	HSA	Dual-modality MRI-MTAI
Yttrium iron garnet (YIG) microparticles	915 MHz <sup>64</sup>			MTAI, in tissue phantoms
Ferromagnetic material-filled multi-walled CNTs (MMWCNTs)	6 GHz <sup>65</sup>	Outer and inner diameter: 30–40, 10–20; lengths: 500–1500		<i>In vivo</i> MTAI of tumors
Anti-Gal1-Fe <sub>3</sub> O <sub>4</sub> nanoparticles	3 GHz <sup>66</sup>	142	Anti-Gal1	<i>In vivo</i> heterozygosity model
Mn <sub>3</sub> O <sub>4</sub>	1.2 GHz <sup>67</sup>	100	RGD	<i>In vivo</i> MTAI of tumors

biocompatible, and electromagnetic properties. The contrast of thersol-gelmoacoustic imaging increases with the concentration of carbonyl iron, which has the ability to improve the contrast and specificity of tissue structure and MTAI. Jin *et al.*<sup>52</sup> obtained spherical particles by simply stabilizing Fe<sub>3</sub>O<sub>4</sub> with citrate, and tested its dielectric constant, calculated its absorption properties with microwave, and performed thermoacoustic imaging. It was found that Fe<sub>3</sub>O<sub>4</sub> nanoprobes have the potential to produce stronger thermoacoustic signals as well as better thermoacoustic imaging results. Another one of the compounds FA-Fe<sub>3</sub>O<sub>4</sub>/PANI<sup>49</sup> is a nanomaterial that couples Fe<sub>3</sub>O<sub>4</sub>/PANI with folic acid (FA). FA-Fe<sub>3</sub>O<sub>4</sub>/PANI can combine with folate receptors *in vivo* to target tumors. Under 6 GHz pulsed microwave conditions, injection of FA-Fe<sub>3</sub>O<sub>4</sub>/PANI showed a higher thermoacoustic signal and better contrast compared to mice injected with Fe<sub>3</sub>O<sub>4</sub>/PANI, while achieving longer elimination time, as shown in Fig. 2(a). Thermoacoustic imaging of functional iron oxide nanomaterials may be useful for tumor-specific targeting and early lesion tissue imaging. Dextran-coated Fe<sub>3</sub>O<sub>4</sub> nanoparticles,<sup>50</sup>

which is a magnetic nanoprobe of iron tetroxide coated by dextrose, showed approximately 4 times higher thermoacoustic signal compared to blood. In addition, there is a significant difference in the intensity of the thermoacoustic signal between the normal hepatic reticuloendothelial system and tumors. Qin *et al.*<sup>51</sup> used dextran-coated Fe<sub>3</sub>O<sub>4</sub> nanoparticles as a contrast agent applied to thermoacoustic tomography for the purpose of detecting hepatocellular carcinoma, which has the potential to become a new method for clinical diagnosis of tumors in the future. Fe<sub>3</sub>O<sub>4</sub>/Au nanoparticles are particles that highly complement Fe<sub>3</sub>O<sub>4</sub> with Au, which can enhance NMR contrast, as well as higher photoacoustic and thermoacoustic signals. Besides, the nanoparticles could specifically target integrin α<sub>v</sub>β<sub>3</sub>-positive cancer cells when attached to FITC-labeled integrin α<sub>v</sub>β<sub>3</sub> mAb and target integrin α<sub>v</sub>β<sub>3</sub>-positive cancer cells when attached to FITC-labeled integrin α<sub>v</sub>β<sub>3</sub> mAb. Hence, Xing *et al.* implemented a bio-modified nanoprobe for cancer cell targeting and tumor imaging, and integrated PAI, MTAI, and NMR imaging into one multimodal imaging, as shown in Fig. 2(b).

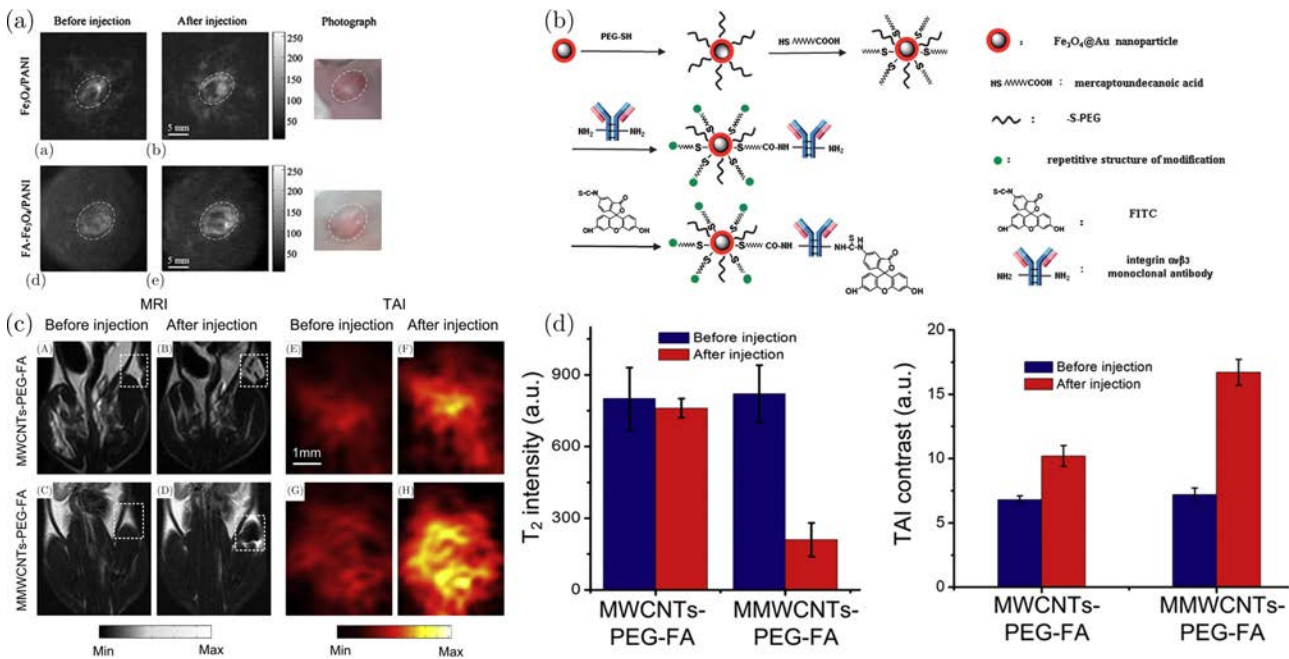


Fig. 2. (a) *In vivo* thermoacoustic imaging of tumors in mice injected with FA-Fe<sub>3</sub>O<sub>4</sub>/PANI.<sup>49</sup> (b) Synthesis process of Fe<sub>3</sub>O<sub>4</sub>/Au nanoparticles.<sup>51</sup> (c), (d) *In vivo* imaging of tumor sections by combining MTAI and NMR imaging systems and MMWCNTs nanomaterials.<sup>65</sup>

In addition to the commonly used Fe<sub>3</sub>O<sub>4</sub> as a magnetic material, MTAI has also attempted with YIG and MMWCNTs, etc. YIG is a magnetic microparticle. Zhang *et al.*<sup>64</sup> combined the ferromagnetic resonance of YIG microparticles with pulsed microwaves for the purpose of enhancing and modulating MTAI. Previously, it has been shown that carbon nanotubes (CNTs) have good electrical and magnetic properties and can be used as contrast agents for MTAI, but they are not well used for the magnetic absorption properties of CNTs. Therefore, Ding *et al.*<sup>65</sup> filled ferromagnetic materials to CNTs for getting MMWCNTs and used folic acid as a targeting molecule connected to multiwalled CNTs (MWCNTs), MMWCNTs. Compared with MWCNTs, MMWCNTs performed for MTAI and NMR imaging can see the size and edges of tumors more clearly, which improves their imaging contrast substantially. MMWCNTs have the potential to become an accurate contrast agent for tumor detection, as shown in Figs. 2(c) and 2(d).

In addition, some researchers have attempted to apply clinically approved exogenous functional nanoparticles to MTAI such as superparamagnetic iron oxide (SPIO) nanoparticles that have been approved for clinical use as ideal NMR contrast agents. In addition, SPIO can resonate in

microwave fields.<sup>68,69</sup> Wen *et al.*<sup>53</sup> used HSA to modify SPIO to obtain HSA-SPIO nanoprobe. The nanoprobe can accurately locate tumor cells using passive targeting and has a strong microwave absorption ability, which has the ability to generate thermoacoustic shock waves to kill cancer cells under the irradiation of pulsed microwaves, in order to achieve the purpose of tumor growth inhibition, showing a better potential for MTA treatment and MTAI. Meanwhile, combined with the advantages of SPIO itself in NMR imaging, it can integrate MTAI and NMR into one to realize dual-modality imaging and combined treatment, thus it is possible to realize precise diagnosis and treatment of tumors, as shown in Fig. 3(a).

MTAI not only has the advantage of deep imaging depth, but also enables identification of deeper and smaller tumors, as well as specific MTAI triggered by the endogenous tumor microenvironment. US imaging and NMR imaging can achieve detection of pancreatic tumors with a minimum diameter of approximately 10 mm. Qin *et al.*<sup>66</sup> found that MTAI can achieve detection of pancreatic tumors with a diameter of less than 5 mm. Qin *et al.* combined galectin-1 antibody (anti-Gal1) with microwave absorber Fe<sub>3</sub>O<sub>4</sub> as anti-Gal1-Fe<sub>3</sub>O<sub>4</sub> nanoparticles for enhancing TA signal and

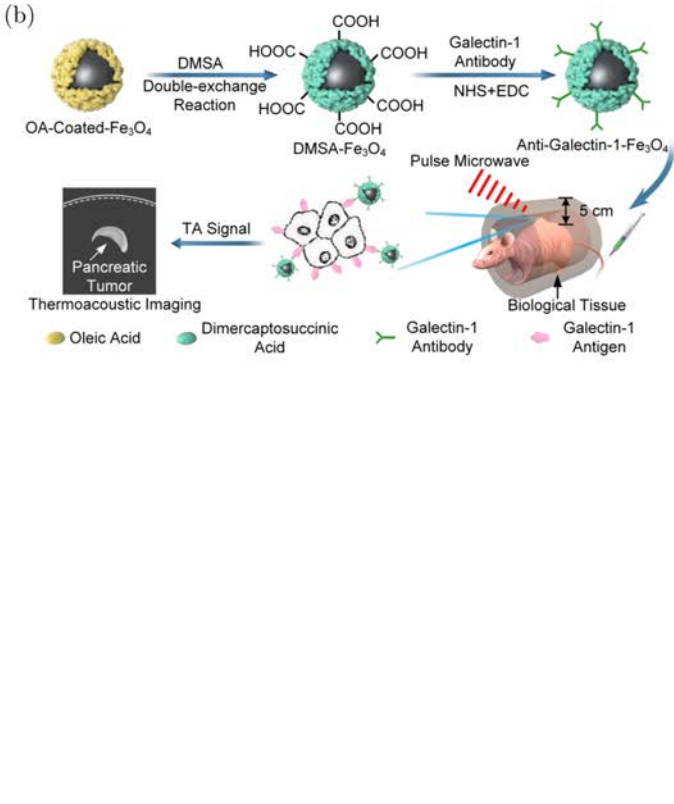
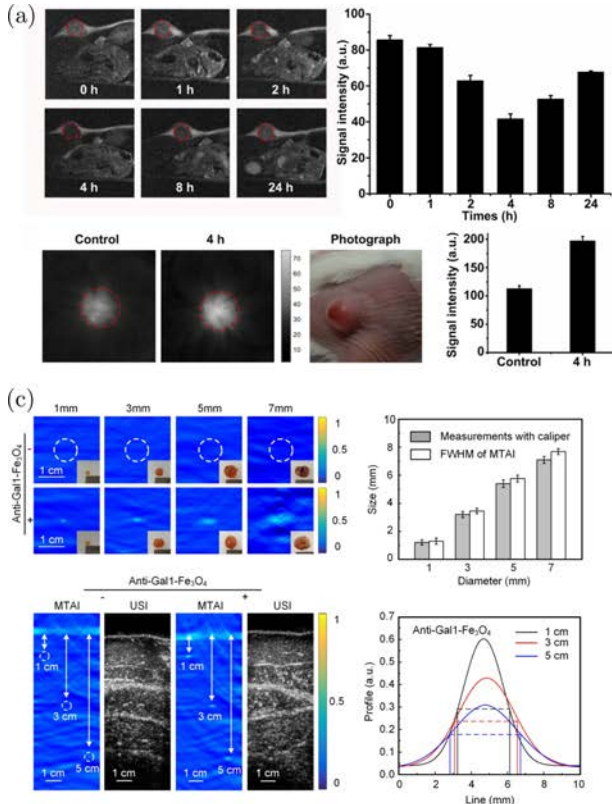


Fig. 3. (a) HSA-SPIO tumor NMR imaging and MTAI in mice.<sup>53</sup> (b) Schematic diagram of the synthesis principle and MTAI of anti-Gal1-Fe<sub>3</sub>O<sub>4</sub> nanoparticles.<sup>66</sup> (c) Anti-Gal1-Fe<sub>3</sub>O<sub>4</sub> nanoparticles for the adjuvant heterozygosity pancreatic cancer model.<sup>66</sup>

enhancing imaging contrast. *In vitro* characterization of the imaging ability of pancreatic tumors with different diameter sizes (1.0 mm, 3.1 mm, 5.0 mm, 7.2 mm in diameter) was performed, and an *in vivo* heterozygosity model was constructed for imaging deep (5 cm) pancreatic tumors (3 mm in diameter) as shown in Figs. 3(b) and 3(c). The feasibility of MTAI to achieve non-invasive *in vivo* detection of small pancreatic tumors was demonstrated in the heterozygosity model. Zhang *et al.*<sup>67</sup> developed a Mn<sub>3</sub>O<sub>4</sub>-PEG (MNP) nanoparticles that can respond to the tumor microenvironment, where overexpressed glutathione and the weak acidity of the tumor microenvironment activate the MNP nanoparticles. It causes the release of Mn<sup>2+</sup> which increases the ion content, so that the highly selective amplification of TA signal in deep tumors is achieved. The MTAI at a depth of 5 cm was also made with good contrast, realizing specific MTAI for deep tumors, as shown in Figs. 4(a) and 4(b).

Besides the metal oxides mentioned above as TA contrast agents, metal nitrides can also achieve a high microwave absorption effect. Although TiN is not a magnetic nanomaterial, TiN is a defect-rich

material. Such a defect-rich TiN nanomaterial was developed by Wu *et al.*<sup>41</sup> This nanomaterial has high dielectric loss and high conductivity loss due to the presence of a large number of local structural defects and carriers, and exhibits better microwave absorption properties. At the depth of 5 cm, it can also have well imaging contrast as shown in Figs. 4(c) and 4(d).

### 2.1.2. Carbon contrast agents

Carbon can form materials with different properties, such as carbon nanotubes, graphene nanomaterials and other materials. Such materials have been widely explored in the recent decade for biological and biomedical applications. Carbon contrast agents possess better microwave absorption due to their high specific surface area, activated carrier mobility or abundant vacancy defects, all of these features can enhance the conductivity loss and polarization loss of carbon contrast agents. For example, single-wall carbon nanotubes (SWNTs) can cross cell membranes without causing cytotoxicity,<sup>70</sup> which has been widely used in novel carriers

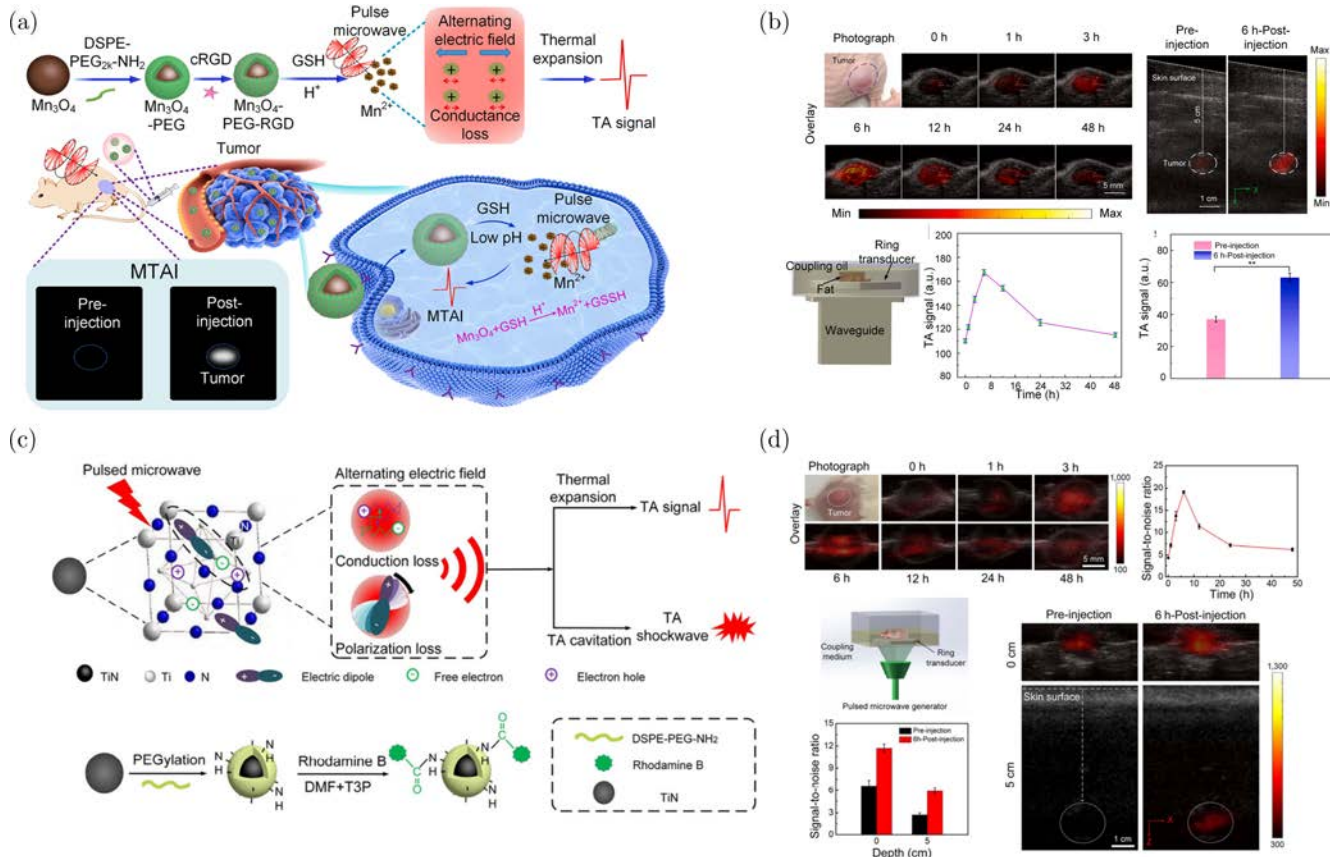


Fig. 4. (a) Schematic diagram of Mn<sub>3</sub>O<sub>4</sub>-PEG-RGD synthesis and TA signaling generation mechanism.<sup>67</sup> (b) Comparison of MTAI of Mn<sub>3</sub>O<sub>4</sub>-PEG-RGD assisted breast tumors in mice.<sup>67</sup> (c) Schematic diagram of the synthesis of defect-rich TiN nanoparticles and the mechanism of TA signaling generation.<sup>41</sup> (d) Comparison of MTAI of TiN nanoparticles assisted mice breast tumors.<sup>41</sup>

such as drugs<sup>71</sup> and proteins.<sup>72</sup> Previous investigations have demonstrated that carbon nanotubes can accumulate in the mitochondria of cancer cells, as well as absorb the energy of microwaves to convert into TA shock waves.<sup>73-75</sup> TA therapy is achieved by disrupting the mitochondria of cancer cells to activate the apoptotic pathway.<sup>76</sup> GO has a variety of physical properties and is the most common derivative of graphene, which has been widely explored in biomedicine and electromagnetic absorption.<sup>77-79</sup> Moreover, the reduced graphene oxide (rGO) obtained by reduction has a high specific surface area, activated carrier mobility and the presence of defects such as missing carbon atoms, thus exhibiting good attenuation capability.<sup>80-82</sup> Meanwhile rGO has been shown to be a very promising microwave absorber.<sup>83-85</sup> Wang *et al.* indicated that graphene with defects would have more vacancy defects and more dielectric loss than graphene oxide, which would have stronger

microwave absorption.<sup>86,87</sup> Yuan *et al.*<sup>40</sup> proposed a technique based on the physical principle that allows the improvement of dielectric loss of nanoparticles by increasing the atomic defects of nanoparticles, which results in the TA signal and MTAI contrast are enhanced. It mainly uses bovine serum albumin (BSA) as a reducing agent to bind GO to BSA by  $\pi-\pi$  superposition. GO reduced by BSA can produce an external vacancy defect, and since the distribution of the electron cloud around the vacancy is inhomogeneous, this defect generates electric dipoles. GO reduced by BSA can produce an external vacancy defect, and since the distribution of the electron cloud around the vacancy is inhomogeneous, this defect generates electric dipoles. Under pulsed microwave irradiation, these electric dipoles are repolarized, resulting in transient heating and thermoelastic expansion, producing the effect of an amplified TA signal, which in turn improves the MTAI contrast, as shown in Figs. 5(a) and 5(b).

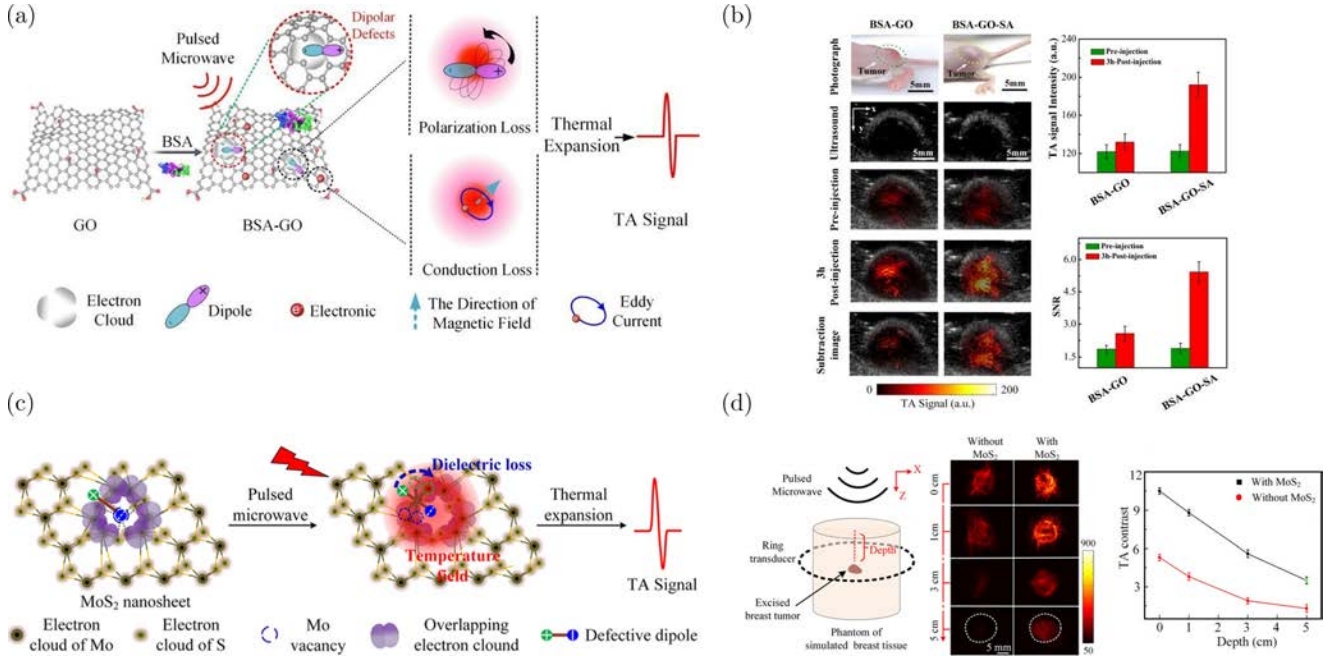


Fig. 5. (a) Schematic diagram of TA signal generation mechanism of BSA-GO nanoparticles.<sup>40</sup> (b) MTAI of BSA-GO-SA tumors in mice *in vivo*.<sup>40</sup> (c) Schematic representation of defect-rich S-MoS<sub>2</sub>-PEG nanosheets generating TA signals.<sup>91</sup> (d) *In vitro* MTAI study of breast tumors located in deep tissues.<sup>91</sup>

With the development of microwave devices and exogenous functional nanoparticles, MTAI not only offers the advantages of high contrast and high resolution, but also TA treatment enables the treatment of multi-locus tumors and tumor metastases. Pramanik *et al.*<sup>88</sup> used SWNTs as a dual-modality contrast agent for MTAI and PA tomography (PAT) dual-modality contrast agents; SWNTs exhibited more than 2 times the signal enhancement in MTAT at 3 GHz compared to blood. Wang *et al.*<sup>89</sup> investigated the thermo-acoustic response properties of carbon nanotubes, which laid the theoretical foundation for the application of carbon-based nanomaterials for MTAI. In addition, Lalwani *et al.*<sup>73</sup> also realized the use of graphene as a contrast agent for MTAT. In TA treatment, Wen *et al.*<sup>76</sup> used mitochondria-targeted SWNTs as microwave absorbers for deep tumor treatment. The SWNTs can effectively absorb ultrashort microwave energy and convert it into TA shock waves to kill the targeted mitochondria, thus inducing apoptosis of cancer cells. TA therapy has the advantage of no significant side effects and also achieves a high cancer cell death rate, which is difficult to be achieved by both photothermal and photoacoustic therapy.

### 2.1.3. Black phosphorus and transition metal sulfide contrast agents

Both transition metal sulfides and BP belong to two-dimensional inorganic nanomaterials, which have been extensively investigated in the fields of material science and biomedicine due to their specificity.<sup>90</sup> These two-dimensional inorganic nanomaterials are prone to atomic vacancies during their preparation,<sup>42,91–95</sup> which have a high number of defective electric dipoles. Under pulsed microwave conditions, these defective electric dipoles are repeatedly polarized, which leads to high dielectric losses, after thermal elastic expansion to achieve energy conversion and generate TA shock waves.<sup>42,91–93</sup> Therefore, the microwave absorption properties of both transition metal sulfides and black phosphorus with atomic vacancies are relatively well. Li *et al.*<sup>91</sup> developed defect-rich single-layer molybdenum disulfide (S-MoS<sub>2</sub>) nanosheets with high dielectric loss. The TA signal was amplified by adjusting the atomic defect rate of the S-MoS<sub>2</sub> nanosheets to make them have higher dielectric loss. The enhancement of the TA signal resulted in the improved contrast of MTAI at deeper depths, as shown in Figs. 5(c)–5(d), where the contrast of MTAI was significantly improved at a

depth of 5 cm. Zhang *et al.*<sup>92</sup> combined perfluorohexane (PFH) and tungsten disulfide ( $\text{WS}_2$ ), the defect-rich  $\text{WS}_2$  was used as a microwave absorber. The TA shock wave generated by the absorption of microwave by  $\text{WS}_2$  makes the PFH droplet undergo liquid–gas phase transition, which results in the amplification of TA signal. A significant enhancement of TA signal can be seen in the MTAI of breast tumors *in vivo*, as shown in Fig. 6(a). Despite the excellent microwave absorption capability of transition metal sulfides, the risk of their accumulation *in vivo* prevents them from being widely used in clinical aspects. The  $\text{Fe}^{3+}$  doped BP ( $\text{BP}_{\text{Fe}(3+)}$ ) developed by Chen *et al.*<sup>42</sup> not only has efficient microwave acoustic conversion capability, but also can be biodegradable, which breaks the limitations of TA contrast agents and has more potential for clinical applications. In  $\text{BP}_{\text{Fe}(3+)}$ ,  $\text{Fe}^{3+}$  adsorbed with the single pair of electrons of BP through conjugated  $\pi$ -bonds, which led to the increase of permanent electric dipole, and the increase of electric dipole made the TA signal enhanced. The contrast of MTAI at the tumor site was significantly improved after injection of  $\text{BP}_{\text{Fe}(3+)}$ @PLGA nanoparticles, moreover, the tumor was obviously suppressed after  $\text{BP}_{\text{Fe}(3+)}$ @PLGA nanoparticles treatment and confirmed by MTAI, as shown in Figs. 6(b)–6(c).

## 2.2. Organic nanomaterials

It has been shown that both amino acid polymers and ionic polymers are biodegradable and have low

toxicity. They have good absorption capacity under pulsed microwaves. For example,  $\text{NMG}_2[\text{Gd}(\text{DTPA})]$  is a paramagnetic ionic contrast agent that has been applied in clinical NMR imaging. Qin *et al.*<sup>30</sup> successfully applied  $\text{NMG}_2[\text{Gd}(\text{DTPA})]$  in MTAI, which is a nanomaterial with seven unpaired electrons in the 4f orbital of  $\text{Gd}^{3+}$ , charged ions  $\text{NMG}^+$ ,  $[\text{Gd}(\text{DTPA})]^{2-}$  and unpaired electrons that can interact with the microwave field. The increase of charged ion concentration of  $\text{NMG}_2[\text{Gd}(\text{DTPA})]$  makes the ion loss increase, which results in the enhancement of its thermoacoustic signal. The experimental results demonstrate that the nanoprobe can make the tumor contour clearer and easier to distinguish from normal tissue in MTAI, as shown in Fig. 7(a). Chen *et al.*<sup>43</sup> used perfluorocarbon as a shell to synthesize engineered saline nanodroplets, which successfully increased the TA signal by hundreds of times using the high conductivity of  $\text{NaCl}$ , as shown in Fig. 7(b).

Among the alkaline amino acids, including lysine, arginine and histidine, all of them are polar molecules.<sup>96</sup> Alkaline amino acid materials have been previously reported in relation to their properties in microwave fields. They can generate electric dipoles under the irradiation of pulsed microwaves for the purpose of absorbing microwave energy.<sup>97</sup> At the same time, the dielectric loss and conductivity of alkaline amino acids will increase with increasing concentration, which will produce a reaction in the electromagnetic field exhibiting electrolytic properties.<sup>96</sup> Under pulsed microwave conditions, the molecular polarization of alkaline amino acids

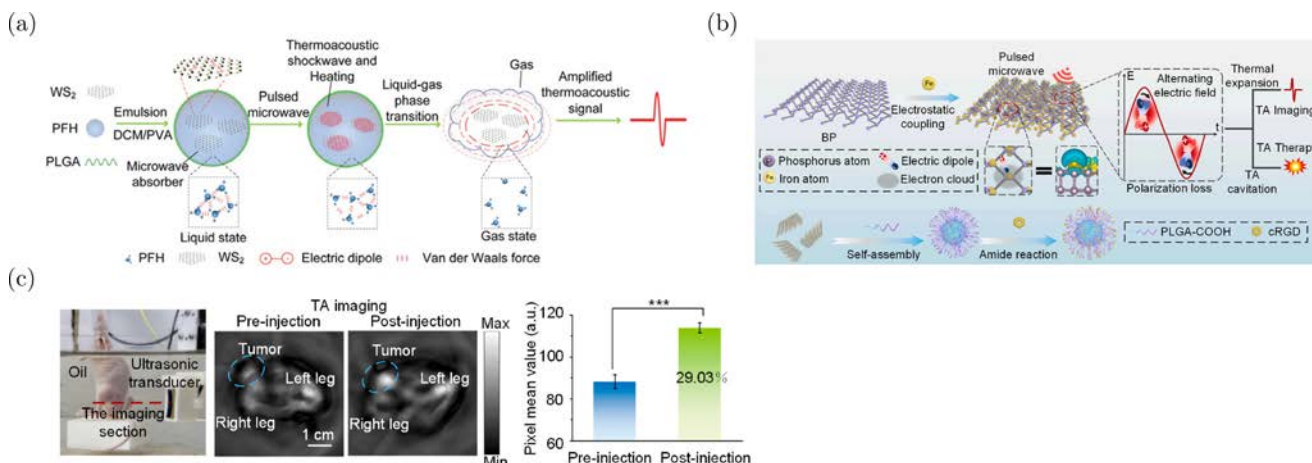


Fig. 6. (a) Schematic diagram of the TA signal amplification mechanism of the liquid–gas phase change nanoprobe.<sup>92</sup> (b) Schematic diagram of the synthesis mechanism and TA signal generation mechanism of  $\text{BP}_{\text{Fe}(3+)}$ @PLGA-RGD.<sup>42</sup> (c) Comparison of  $\text{BP}_{\text{Fe}(3+)}$ @PLGA-RGD-assisted MTAI using a single array ring scan system with imaging cross-sections shown as red dashed lines.<sup>42</sup>

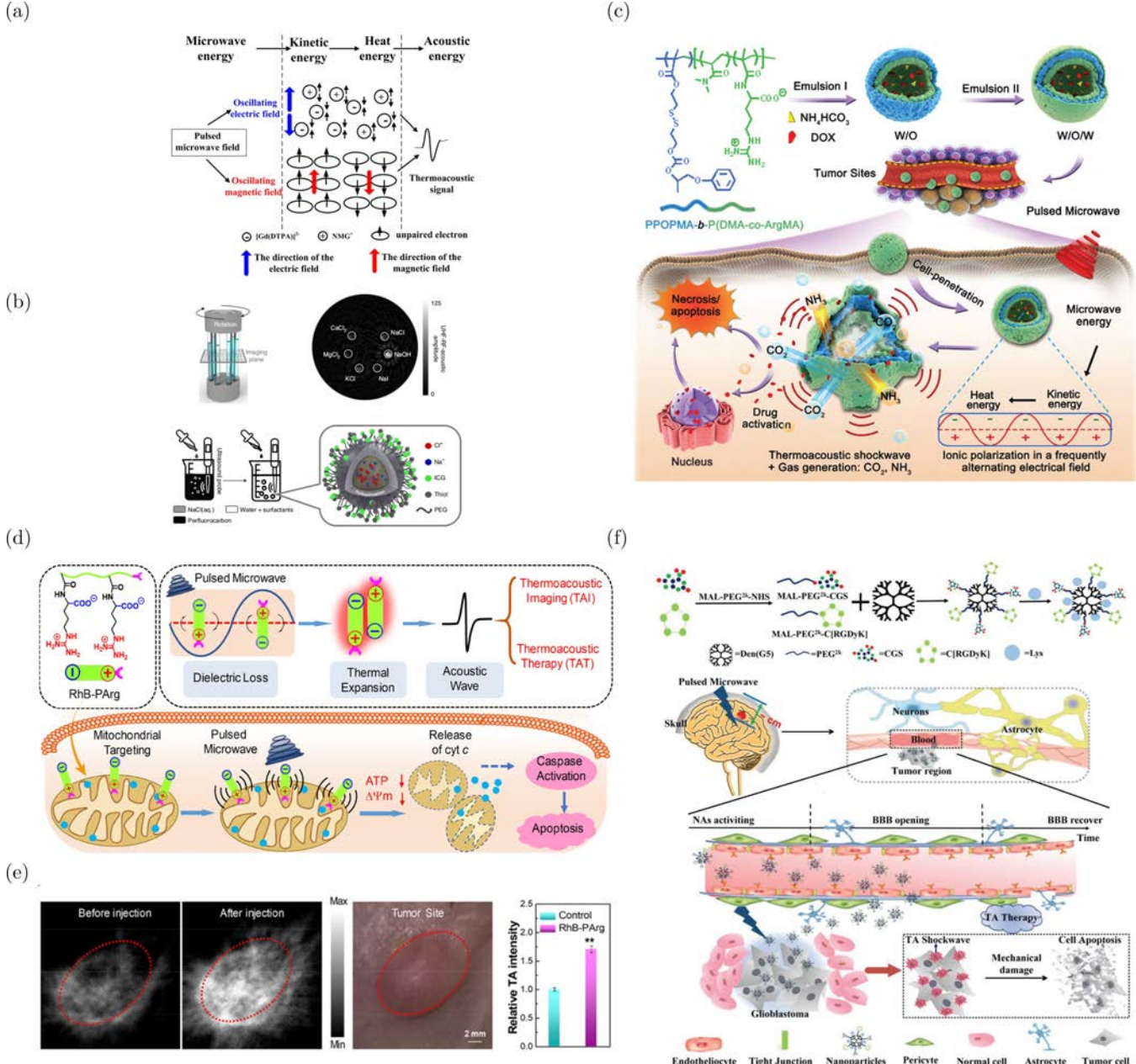


Fig. 7. (a) Schematic diagram of TA signal generation theory of NMG<sub>2</sub>[Gd(DTPA)] nanoparticles.<sup>30</sup> (b) Schematic diagram of engineered saline nanodroplets preparation and *in vitro* imaging.<sup>43</sup> (c) Schematic diagram of highly exploitable nanocapsules and fabrication of pulsed microwave triggered intracellular thermal cavitation, gas burst and drug release.<sup>99</sup> (d) Schematic diagram of RhB-PArg nanomaterials for thermoacoustic imaging and thermoacoustic therapy.<sup>100</sup> (e) TA intensity at the tumor site after RhB-PArg injection in mice.<sup>101</sup> (f) Schematic diagram of synthesis and TA treatment of Den-CGS/RGD/Lys nanoparticles.<sup>101</sup>

increases, the dipole motion increases resulting in enhanced collisions with other dipoles, allowing the conversion of microwave energy into thermal energy, the instantaneous temperature rise causes a thermal expansion effect, which eventually generates TA shock waves.<sup>98</sup> This provides a theoretical basis for the application of alkaline amino acids

in pulsed microwaves, making them available for MTAI and TA therapy.

Wang *et al.*<sup>99</sup> prepared P(ArgMA-co-DMA)-*b*-PPOPMA, arginine-tethered reduction-responsive copolymers, ammonium bicarbonate and doxorubicin into nanocapsules, which were irradiated by pulsed microwaves and caused TA shock waves.

The nanocapsules are irradiated by pulsed microwaves, which absorb microwave energy and cause TA shock waves, meanwhile its ammonium bicarbonate is decomposed to carbon dioxide and ammonia thereby enhancing the thermoacoustic cavitation effect. The TA shock wave causes damage to the cells, while the nanocapsules also release the carried doxorubicin into the cells, eventually causing cell death, as shown in Fig. 7(c). Zhai *et al.*<sup>100</sup> obtained drug-free RhB-PArg nanomaterials with mitochondrial targeting by preparing them with arginine monomer (Arg) and rhodamine B (RhB). Since RhB-PArg has a negatively charged carboxyl group and a positively charged guanidine group on part of its side chain, it can exhibit obvious properties of electrolysis, which makes it better able to absorb the pulsed microwave energy and the generated TA signal. RhB-PArg not only has a high therapeutic efficiency, but also has a significant improvement in MTAI contrast, as shown in Figs. 7(d)–7(e). Moreover, Li *et al.*<sup>101</sup> composed a thermoacoustic probe by using polar amino acids and adenosine-based agonists, which can efficiently absorb microwave energy as well as have the ability to penetrate the blood–brain barrier (BBB) at the tumor site. This thermoacoustic probe activates the adenosine receptors of the BBB via adenosine-based agonists, allowing the thermoacoustic probe to pass through the BBB and accumulate in glioblastomas. Meanwhile, the thermoacoustic cavitation effect generated by the thermoacoustic probe can mechanically destroy the tumor cells in a short period of time with minimal damage to the surrounding normal brain tissue, as shown in Fig. 7(f).

### 3. Discussion

MTAI combined with contrast agents can provide more innovative opportunities in early diagnosis, more accurate tumor localization, drug delivery and monitoring, targeted tumor therapy, intraoperative navigation, and other applications, as well as a future trend. Although MTAI technology can achieve high contrast, high-resolution, and high-sensitivity deep tumor imaging, it has not really achieved clinical translation compared with US imaging, PAI, and NMR imaging. MTAI technology still faces barriers in equipment miniaturization and integration, which needs continued optimization in image reconstruction algorithms and imaging speed to achieve the desired state. Improving the contrast

of MTAI also requires continued development of more efficient contrast agents, as well as attempts to use multiple frequencies of microwaves for excitation, resulting in high-sensitivity and high contrast MTAI. In addition to high efficiency, the development of contrast agents needs to have appropriate biocompatibility and low biotoxicity, complete dissolution *in vivo*, good stability, low cost, and long half-life, etc. This paper reviews the current progress of TA contrast agents in MTAI and MTA therapy. Some research studies have shown that MTAI uses exogenous functional nanoparticles that can achieve better biocompatibility and lower biotoxicity, such as biodegradable BP, amino acids materials and engineered saline nanodroplets nanomaterials, but there is still the disadvantage of higher production cost. Although the current microwave absorbers can achieve MTAI and certain therapeutic effect, they have not really achieved clinical transition. There is still a need to explore higher MTA conversion efficiency and higher biosafety nanomaterials to achieve a safer, deeper and more effective MTAI and MTA therapy.

In fact, although many researchers have made a lot of efforts in developing new TA contrast agents, which have achieved better imaging and therapeutic effects in breast cancer, glioblastoma, pancreatic cancer, etc., the related research is still in the primary stage and needs to be continuously approached in the direction of clinical translation. In short, there is still a need to continuously develop exogenous functional nanoparticles with good biosafety, strong microwave absorption and good targeting. By combining MTAI with exogenous functional nanoparticles, the gap between MTAI and clinical applications can be narrowed as much as possible to promote the development of precise and efficient treatment of tumors.

### Acknowledgments

This research was supported by the National Natural Science Foundation of China (62075066); the Science and Technology Planning Project of Guangdong Province, China (2019A1515012054); the Science and Technology Program of Guangzhou (2019050001); the Science and Technology Program of Guangzhou (202201010718); and the Key-Area Research and Development Program of Guangdong Province (2019B030335001).

## Conflicts of Interest

The authors declare that there are no conflicts of interest relevant to this article.

## References

1. B. Brooksby, B. W. Pogue, S. D. Jiang, H. Dehghani, S. Srinivasan, C. Kogel, T. Tosteson, J. Weaver, S. Poplack, K. Paulsen, "Imaging breast adipose and fibroglandular tissue molecular signatures by using hybrid MRI-guided near-infrared spectral tomography," *Proc. Natl. Acad. Sci.* **103**, 8828 (2006).
2. M. Bendszus, C. Wessig, L. Solymosi, K. Reiners, M. Koltzenburg, "MRI of peripheral nerve degeneration and regeneration: correlation with electrophysiology and histology," *Exp. Neurol.* **188**, 171–177 (2004).
3. H. Kramer, P. J. Pickhardt, M. A. Kliewer, D. Hernando, G. H. Chen, J. A. Zagzebski, S. B. Reeder, "Accuracy of liver fat quantification with advanced ct, mri, and ultrasound techniques: prospective comparison with MR spectroscopy," *AJR.* **208**, 92–100 (2017).
4. A. Pizurica, A. M. Wink, E. Vansteenkiste, W. Philips, B. J. Roerdink, "A review of wavelet denoising in MRI and ultrasound brain imaging," *Curr. Med. Imaging Rev.* **2**, 247–260 (2006).
5. B. D. Pooler, C. N. Wiens, A. Mcmillan, N. S. Artz, A. Schlein, Y. Covarrubias, J. Hooker, J. B. Schwimmer, L. M. Funk, G. M. Campos, J. A. Greenberg, G. Jacobsen, S. Horgan, T. Wolfson, A. C. Gamst, C. B. Sirlin, S. B. Reeder, "Monitoring fatty liver disease with MRI following bariatric surgery: a prospective, dual-center study," *Radiology* **290**, 682–690 (2019).
6. P. Strax, "Detection of breast cancer," *Cancer* **66**, 1336–1340 (1990).
7. A. Sakdinawat, D. Attwood, "Nanoscale X-ray imaging," *Nat. Photonics.* **4**, 840–8 (2010).
8. F. Pfeiffer, M. Bech, O. Bunk, P. Kraft, E. F. Eikenberry, Ch. Brönnimann, C. Grünzweig, C. David, "Hard-X-ray dark-field imaging using a grating interferometer," *Nat. Mater.* **7**, 134–137 (2008).
9. D. Chapman, W. Thominson, R. E. Johnston, D. Washburn, E. Pisano, N. Gmür, Z. Zhong, R. Menk, F. Arfelli, D. Sayers, "Diffraction enhanced X-ray imaging," *Phys. Med. Biol.* **42**, 2015–2025 (1997).
10. P. E. Freer, "Mammographic breast density: impact on breast cancer risk and implications for screening," *RadioGraphics* **35**, 302–315 (2015).
11. R. W. Pinsky, M. A. Helvie, "Mammographic breast density: effect on imaging and breast cancer risk," *J. Nat. Compr. Canc. Netw.* **8**, 1157–1165 (2010).
12. W. Teh, A. Wilson, "The role of ultrasound in breast cancer screening. A consensus statement by the european group for breast cancer screening," *Eur. J. Cancer.* **34**, 449–450 (1998).
13. N. Duric, P. Littrup, A. Babkin, D. Chambers, S. Azevedo, A. Kalinin, R. Pevzner, M. Tokarev, E. Holsapple, O. Rama, R. Duncan, "Development of ultrasound tomography for breast imaging: technical assessment," *Med. Phys.* **32**, 1375–1386 (2005).
14. K. Hyynnen, G. T. Clement, N. McDannold, N. Vykhodtseva, R. King, P. J. White, S. Vitek, F. A. Jolesz, "500-element ultrasound phased array system for noninvasive focal surgery of the brain: a preliminary rabbit study with *ex vivo* human skulls," *Magn. Reson. Med.* **52**, 100–107 (2004).
15. J. F. Synnevag, A. Austeng, S. Holm, "Adaptive beamforming applied to medical ultrasound imaging," *IEEE Trans. Ultrason. Ferroelectr. Freq. Control* **54**, 1606–1613 (2007).
16. J. Bamber, D. Cosgrove, C. F. Dietrich, J. Fro mageau, J. Bojunga, F. Calliada, V. Cantisani, J. M. Correas, M. D'Onofrio, E. E. Drakonaki, M. Fink, M. Friedrich-Rust, O. H. Gilja, R. F. Havre, C. Jenssen, A. S. Klauser, R. Ohlinger, A. Saftoiu, F. Schaefer, I. Sporea, F. Piscaglia, "EFSUMB guidelines and recommendations on the clinical use of ultrasound elastography. Part 1: basic principles and technology," *Ultraschall Med.* **34**, 169–184 (2013).
17. M. Tanter, M. Fink, "Ultrafast imaging in biomedical ultrasound," *IEEE Trans. Ultrason. Ferroelectr. Freq. Control* **61**, 102–119 (2014).
18. U. Zaleska-Dorobisz, K. Kaczorowski, A. Pawlus, A. Puchalska, M. Inglot, "Ultrasound elastography-review of techniques and its clinical applications," *Adv. Clin. Exp. Med.* **23**, 645–655 (2014).
19. R. J. Hooley, L. M. Scoutt, L. E. Philpotts, "Breast ultrasonography: state of the art," *Radiology* **268**, 642–659 (2013).
20. D. Huang, E. Swanson, C. Lin, J. S. Schuman, W. G. Stinson, W. Chang, M. R. Hee, T. Flotte, K. Gregory, C. A. Puliafito, J. G. Fujimoto, "Optical coherence tomography," *Science* **254**, 1178–1181 (1991).
21. X. Gu, Y. Xu, H. Jiang, "Mesh-based enhancement schemes in diffuse optical tomography," *Med. Phys.* **30**, 861–869 (2003).
22. K. X. Deng, M. X. Cui, H. Z. Zuo, X. H. Wang, C. J. Cai, J. W. Luo, C. Ma, "Speed-of-sound

- heterogeneity compensation method in photoacoustic computed tomographic image reconstruction," *Chin. J. Lasers* **48**, 1507001 (2021).
23. J. Li, S. C. Miao, S. Z. Song, T. Lu, T. T. Chen, F. Gao, "Reconstruction algorithm based on a virtual parallel-projection model for photoacoustic tomography using an ultrasonic transducer with a large active surface," *Chin. J. Lasers* **48**, 1607001 (2021).
  24. K. Xu, C. Wang, M. J. Zhang, Q. Cheng, H. Z. Xiang, G. Zheng, "Photoacoustic spectrum analysis of atherosclerotic vessels," *Laser Optoelectron. Pro.* **58**, 1217001 (2021).
  25. Q. S. Lu, L. H. Jin, Y. K. Xu, "Progress on applications of deep learning in super-resolution microscopy imaging," *Laser Optoelectron. Pro.* **58**, 2400007 (2021).
  26. X. Wang, S. J. Tu, X. Liu, Y. H. Zhao, C. F. Kuang, X. Liu, X. Hao, "Advance and prospect for three-dimensional super-resolution microscopy," *Laser Optoelectron. Pro.* **58**, 2200001 (2021).
  27. A. B. Milstein, S. Oh, K. J. Webb, C. A. Bouman, Q. Zhang, D. A. Boas, R. P. Millane, "Fluorescence optical diffusion tomography," *Appl. Opt.* **42**, 3081–3094 (2003).
  28. A. G. Bell, "On the production and reproduction of sound by light," *Am. J. Sci.* **20**, 305–324 (1880).
  29. T. Bowen, "Radiation-induced thermoacoustic soft tissue imaging," *Ultrason. Symp.* 14–16 (1981).
  30. H. Qin, S. Yang, D. Xing, "Microwave-induced thermoacoustic computed tomography with a clinical contrast agent of NMG<sub>2</sub>[Gd(DTPA)]," *Appl. Phys. Lett.* **100**, 033701 (2012).
  31. S. X. Zhang, X. Y. Tang, H. Qin, "Research progress and prospect of microwave-induced thermoacoustic imaging technology," *Laser Optoelectron. Prog.* **59**, 0617004 (2022).
  32. Z. Liang, W. P. Wang, S. Q. Qiao, L. Huang, "Study on response of metal wire in thermoacoustic imaging," *J. Innov. Opt. Heal. Sci.* **15**, 2250015 (2022).
  33. R. Rahpeimaa, M. Soltanibcdef, F. M. Kashkoolbg, "Numerical study of microwave induced thermoacoustic imaging for initial detection of cancer of breast on anatomically realistic breast phantom," *Comput. Meth. Prog. Bio.* **196**, 105606 (2020).
  34. Y. J. Li, S. X. Zhang, L. H. Wu, Z. W. Cheng, Z. H. Zhang, H. H. Wang, S. X. Zhao, M. Y. Ren, S. H. Yang, D. Xing, H. Qin, "Polarization microwave-induced thermoacoustic imaging for quantitative characterization of deep biological tissue microstructures," *Photonics Res.* **10**, 1297–1306 (2022).
  35. L. Huang, L. Yao, L. X. Liu, J. Rong, H. Jiang, "Quantitative thermoacoustic tomography: recovery of conductivity maps of heterogeneous media," *Appl. Phys. Lett.* **101**, 244106 (2012).
  36. M. Lazebnik, D. Popovic, L. McCartney, C. B. Watkins, M. J. Lindstrom, J. Harter, S. Sewall, T. Ogilvie, A. Magliocco, T. M. Breslin, W. Temple, D. Mew, J. H. Booske, M. Okoniewski, S. C. Hagness, "A large-scale study of the ultrawideband microwave dielectric properties of normal, benign and malignant breast tissues obtained from cancer surgeries," *Phys. Med. Biol.* **52**, 6093–6115 (2007).
  37. S. Gabriel, R. W. Lau, C. Gabriel, "The dielectric properties of biological tissues: III. Parametric models for the dielectric spectrum of tissues," *Phys. Med. Biol.* **41**, 2271–2293 (1996).
  38. W. T. Joines, Y. Zhang, C. Li, R. Jirtle, "The measured electrical properties of normal and malignant human tissues from 50 to 900 MHz," *Med. Phys.* **21**, 547–550 (1994).
  39. A. Jonscher, "Physical basis of dielectric loss," *Nature* **253**, 717–719 (1975).
  40. C. Yuan, B. H. Qin, H. Qin, D. Xing, "Increasing dielectric loss of a graphene oxide nanoparticle to enhance the microwave thermoacoustic imaging contrast of breast tumor," *Nanoscale* **11**, 22222–22229 (2019).
  41. Z. Wu, F. Zeng, L. Zhang, S. Zhao, L. Wu, H. Qin, D. Xing, "Defect-rich titanium nitride nanoparticle with high microwave-acoustic conversion efficiency for thermoacoustic imaging-guided deep tumor therapy," *Nano Res.* **14**, 2717–2727 (2020).
  42. X. Chen, S. Zhang, J. Liu, M. Ren, D. Xing, H. Qin, "Controlling dielectric loss of biodegradable black phosphorus nanosheets by iron-ion-modification for imaging-guided microwave thermoacoustic therapy," *Biomaterials* **287**, 121662 (2022).
  43. Y. S. Chen, Y. Zhao, C. Beinat, A. Zlitni, E. C. Hsu, D. H. Chen, F. Achterberg, H. Wang, T. Stoyanova, J. Dionne, S. S. Gambhir, "Ultra-high-frequency radio-frequency acoustic molecular imaging with saline nanodroplets in living subjects," *Nat Nanotechnol.* **16**, 717–724 (2021).
  44. K. Yu, S. Wang, Q. Li, T. T. Hou, Y. Xin, R. He, W. H. Zhang, S. Q. Liang, L. B. Wang, W. K. Zhu, "Au atoms doped in Ti<sub>3</sub>C<sub>2</sub>T<sub>x</sub> MXene: Benefiting recovery of oxygen vacancies towards photocatalytic aerobic oxidation," *Nano Res.* **15**, 2862–9 (2022).
  45. M. Q. Huang, L. Wang, W. B. You, R. C. Che, "Single zinc atoms anchored on MOF-derived N-doped carbon shell cooperated with magnetic core as an ultrawideband microwave absorber," *Small* **17**, 2101416 (2021).

46. R. D. Guo, G. L. Yu, M. M. Zhu, Y. Qiu, G. H. Wu, H. M. Zhou, "Regulation of magnetic and electrical performances in core-shell-structured FeSiCr@BaTiO<sub>3</sub> soft magnetic composites," *J. Alloys Compd.* **895**, 162724 (2022).
47. I. Morales, R. Costo, N. Mille, G. Silva, J. Carrey, A. Hernando, P. Presa, "High frequency hysteresis losses on  $\gamma$ -Fe<sub>2</sub>O<sub>3</sub> and Fe<sub>3</sub>O<sub>4</sub>: Susceptibility as a magnetic stamp for chain formation," *Nanomaterials* **8**, 970 (2018).
48. P. J. Sugumaran, Y. Yang, Y. Wang, X. Liu, J. Ding, "Influence of the aspect ratio of iron oxide nanorods on hysteresis-loss-mediated magnetic hyperthermia," *ACS Appl. Bio Mater.* **4**, 4809–4820 (2021).
49. L. Nie, Z. Ou, S. Yang, D. Xing, "Thermoacoustic molecular tomography with magnetic nanoparticle contrast agents for targeted tumor detection," *Med. Phys.* **37**, 4193–4200 (2010).
50. H. Qin, D. Xu, S. Yang, "Dextran-coated Fe<sub>3</sub>O<sub>4</sub> magnetic nanoparticles as a contrast agent in thermoacoustic tomography for hepatocellular carcinoma detection," *J. Phys.* **277**, 12028–12034 (2011).
51. T. Zhou, B. Wu, D. Xing, "Bio-modified Fe<sub>3</sub>O<sub>4</sub> core/Au shell nanoparticles for targeting and multimodal imaging of cancer cells," *J. Mater. Chem.* **22**, 470–477 (2012).
52. X. Jin, A. Keho, K. Meissner, L. V. Wang, "Iron-oxide nanoparticles as a contrast agent in thermoacoustic tomography," *Photons Plus Ultrasound: Imaging Sen.* (2007).
53. L. Wen, S. Yang, J. Zhong, D. Xing, "Thermoacoustic imaging and therapy guidance based on ultra-short pulsed microwave pumped thermoelastic effect induced with superparamagnetic iron oxide nanoparticles," *Theranostics* **7**, 1976–1989 (2017).
54. Z. Chi, Y. Zhao, J. Yang, T. Li, G. Zhang, H. Jiang, "Thermoacoustic tomography of *in vivo* human finger joints," *IEEE Trans. Biomed. Eng.* **66**, 1598–1608 (2019).
55. A. Yan, L. Lin, C. Liu, J. Shi, S. Na, L. V. Wang, "Microwave-induced thermoacoustic tomography through an adult human skull," *Med. Phys.* **46**, 1793–1797 (2019).
56. X. Liang, H. Guo, Q. Liu, C. Wu, Y. Gong, L. Xi, "Thermoacoustic endoscopy," *Appl. Phys. Lett.* **116**, 013702 (2020).
57. M. S. Aliroteh, A. Arbabian, "Microwave-induced thermoacoustic imaging of subcutaneous vasculature with near-field RF excitation," *IEEE Trans. Ultrason. Ferroelectr. Freq. Control* **66**, 577–588 (2018).
58. D. Wu, L. Huang, M. S. Jiang, H. B. Jiang, "Contrast agents for photoacoustic and thermoacoustic imaging: a review," *Int. J. Mol. Sci.* **15**, 23616–23639 (2014).
59. H. B. Jiang, *Thermoacoustic Tomography Principles and Applications*, Institute of Physics Publishing, United Kingdom (2020).
60. Z. Chi, L. Huang, S. Ge, H. B. Jiang, "Technical note: anti-phase microwave illumination-based thermoacoustic tomography of *in vivo* human finger joints," *Med. Phys.* **46**, 2363–2369 (2019).
61. G. Ku, B. D. Fornage, X. Jin, M. Xu, K. K. Hunt, L. V. Wang, "Thermoacoustic and photoacoustic tomography of thick biological tissues toward breast imaging," *Technol. Cancer Res. Treat.* **4**, 559–566 (2005).
62. Z. Ji, C. Lou, S. Yang, D. Xing, "Three-dimensional thermoacoustic imaging for early breast cancer detection," *Med. Phys.* **39**, 6738–6744 (2012).
63. L. Nie, D. Xing, D. Yang, L. Zeng, "Microwave-induced thermoacoustic imaging enhanced with a microwave contrast agent," *IEEE-ICME* 23–27 (2007).
64. D. Zhang, B. Wang, X. Wang, "Enhanced and modulated microwave-induced thermoacoustic imaging by ferromagnetic resonance," *Appl. Phys. Express.* (2019).
65. W. Ding, C. Lou, J. Qiu, Z. Zhao, Q. Zhou, M. Liang, Z. Ji, S. H. Yang, D. Xing, "Targeted Fe-filled carbon nanotube as a multifunctional contrast agent for thermoacoustic and magnetic resonance imaging of tumor in living mice," *Nanomedicine* **12**, 235–244 (2016).
66. H. Qin, B. Qin, C. Yuan, Q. Chen, D. Xing, "Pancreatic cancer detection via galectin-1-targeted thermoacoustic imaging: validation in an *in vivo* heterozygosity model," *Theranostics* **10**, 9172–9185 (2020).
67. S. Zhang, W. Li, X. Chen, M. Ren, H. Zhang, D. Xing, H. Qin, "Manganous-manganic oxide nanoparticle as an activatable microwave-induced thermoacoustic probe for deep-located tumor specific imaging *in vivo*," *Photoacoustics* **26**, 100347 (2022).
68. D. K. Kim, M. S. Amin, S. Elborai, S. H. Lee, Y. Koseoglu, M. Zahn, M. Muhammed, "Energy absorption of superparamagnetic iron oxide nanoparticles by microwave irradiation," *J. Appl. Phys.* **97**, 413 (2005).
69. S. Ni, S. Lin, Q. Pan, F. Yang, K. Huang, D. He, "Hydrothermal synthesis and microwave absorption properties of Fe<sub>3</sub>O<sub>4</sub> nanocrystals," *J. Phys. D: Appl. Phys.* **42**, 05504 (2009).

70. A. E. Porter, M. Gass, K. Muller, J. N. Skepper, P. A. Midgley, M. Welland, "Direct imaging of single-walled carbon nanotubes in cells," *Nat. Nanotechnol.* **2**, 713–717 (2007).
71. Z. Liu, K. Chen, C. Davis, S. Sherlock, Q. Z. Cao, X. Y. Chen, H. Dai, "Drug delivery with carbon nanotubes for *in vivo* cancer treatment," *Cancer Res.* **68**, 6652–6660 (2008).
72. N. W. S. Kam, T. C. Jessop, P. A. Wender, H. J. Dai, "Nanotube molecular transporters: internalization of carbon nanotube-protein conjugates into mammalian cells," *J. Am. Chem. Soc.* **126**, 6850–6851 (2004).
73. G. Lalwani, X. Cai, L. Nie, L. V. Wang, B. Sitharaman, "Graphene-based contrast agents for photoacoustic and thermoacoustic tomography," *Photoacoustics* **1**, 62–67 (2013).
74. C. A. Grimes, C. Mungle, D. Kouzoudis, S. Fang, P. C. Eklund, "The 500 MHz to 5.50 GHz complex permittivity spectra of single-wall carbon nanotube-loaded polymer composites," *Chem. Phys. Lett.* **319**, 460–464 (2000).
75. Z. F. Liu, G. Bai, Y. Huang, F. F. Li, Y. F. Ma, T. Y. Guo, X. B. He, X. Lin, H. J. Gao, Y. S. Chen, "Microwave absorption of single-walled carbon nanotubes/soluble cross-linked polyurethane composites," *J. Phys. Chem. C* **111**, 13696–13700 (2007).
76. L. W. Wen, W. Z. Ding, S. H. Yang, D. Xing, "Microwave pumped high-efficient thermoacoustic tumor therapy with single wall carbon nanotubes," *Biomaterials* **75**, 163–173 (2016).
77. J. S. Hua, Y. X. Li, X. Y. Liu, X. X. Li, S. L. Lin, J. L. Gu, "Graphene/MWNT/poly(p-phenylenebenzobisoxazole) multiphase nanocomposite via solution prepolymerization with superior microwave absorption properties and thermal stability," *J. Phys. Chem. C* **121**, 1072 (2017).
78. D. X. Yan, H. Pang, B. Li, R. Vajtai, L. Xu, P. Ren, "Structured reduced graphene oxide/polymer composites for ultra-efficient electromagnetic interference shielding," *Adv. Funct. Mater.* **25**, 559 (2015).
79. W. J. Chen, S. K. Ozdemir, G. M. Zhao, J. Wiersig, L. Yang, "Exceptional points enhance sensing in an optical microcavity," *Nature* **548**, 192–196 (2017).
80. F. Banhart, J. Kotakoski, A. V. Krasheninnikov, "Structural defects in graphene," *ACS Nano* **5**, 26–41 (2010).
81. R. Beams, L. G. Cançado, L. Novotny, "Raman characterization of defects and dopants in graphene," *J. Phys. Condens. Matter.* **27**, 083002 (2015).
82. L. Vicarelli, S. J. Heerema, C. Dekker, H. W. Zandbergen, "Controlling defects in graphene for optimizing the electrical properties of graphene nanodevices," *ACS nano* **9**, 3428–3425 (2015).
83. H. Lv, Y. Guo, Y. Zhao, H. Zhang, B. Zhang, G. Ji, Z. Xu, "Achieving tunable electromagnetic absorber via graphene/carbon sphere composites," *Carbon* **110**, 130–137 (2016).
84. P. Liu, Z. Yao, J. Zhou, Z. Yang, L. B. Kong, "Small magnetic Co-doped NiZn ferrite/graphene nanocomposites and their dual-region microwave absorption performance," *J. Mater. Chem. C* **4**, 9738–9749 (2016).
85. F. Wu, Y. Xia, Y. Wang, M. Wang, "Two-step reduction of self-assembled three-dimensional (3D) reduced graphene oxide (RGO)/zinc oxide (ZnO) nanocomposites for electromagnetic absorption," *J. Mater. Chem. A* **2**, 20307–20315 (2014).
86. C. Wang, X. Han, P. Xu, X. Zhang, Y. Du, S. Hu, X. Wang, "The electromagnetic property of chemically reduced graphene oxide and its application as microwave absorbing material," *Appl. Phys. Lett.* **98**, 072906 (2011).
87. E. Stratakis, K. Savva, D. Konios, C. Petridis, E. Kymakis, "Improving the efficiency of organic photovoltaics by tuning the work function of graphene oxide hole transporting layers," *Nanoscale* **6**, 6925–6931 (2014).
88. M. Pramanik, M. Swierczewska, D. Green, B. Sitharaman, L. V. Wang, "Single-walled carbon nanotubes as a multimodal-thermoacoustic and photoacoustic contrast agent," *J. Biomed. Opt.* **14**, 034018 (2009).
89. X. Wang, R. S. Witte, H. Xin, "Thermoacoustic and photoacoustic characterizations of few-layer graphene by pulsed excitations," *Appl. Phys. Lett.* **108**, 143104 (2016).
90. L. Cheng, J. Liu, X. Gu, H. Gong, X. Shi, T. Liu, C. Wang, X. Wang, G. Liu, H. Xing, W. Bu, B. Sun, Z. Liu, "PEGylated WS<sub>2</sub> nanosheets as a multifunctional theranostic agent for *in vivo* dual-modal CT/photoacoustic imaging guided photothermal therapy," *Adv. Mater.* **26**, 1886–1893 (2014).
91. Y. Li, Q. Tan, H. Qin, D. Xing, "Defect-rich single-layer MoS<sub>2</sub> nanosheets with high dielectric-loss for contrast-enhanced thermoacoustic imaging of breast tumor," *Appl. Phys. Lett.* **115**, 073701 (2019).
92. L. Zhang, H. Qin, F. Zeng, Z. Wu, L. Wu, S. Zhao, D. Xing, "A stimulated liquid-gas phase transition nanoprobe dedicated to enhance the microwave thermoacoustic imaging contrast of breast tumors," *Nanoscale* **12**, 16034–16040 (2020).
93. W. Fang, Y. Shi, D. Xing, "Vacancy-defect-dipole amplifies the thermoacoustic conversion efficiency

- of carbon nanoprobes,” *Nano Res.* **13**, 2413–2419 (2020).
94. D. Le, T. B. Rawal, T. S. Rahman, “Single-layer MoS<sub>2</sub> with sulfur vacancies: structure and catalytic application,” *J. Phys. Chem. C* **118**, 5346–5351 (2014).
95. J. F. Xie, H. Zhang, S. Li, R. Wang, X. Sun, M. Zhou, J. Zhou, X. W. Lou, Y. Xie, “Defect-rich MoS<sub>2</sub> ultrathin nanosheets with additional active edge sites for enhanced electrocatalytic hydrogen evolution,” *Adv. Mater.* **25**, 5807–5813 (2013).
96. C. Meng, F. Da-Ming, H. Lue-Lue, G. Yi-Shu, H. Jian-Lian, Z. Jian-Xin, Z. Hao, “A new approach to microwave food research: analyzing the electromagnetic response of basic amino acids,” *Innov. Food Sci. Emerg. Technol.* **41**, 100–108 (2017).
97. W. L. Luo, Z. Ji, S. H. Yang, D. Xing, “Microwave-pumped electric-dipole resonance absorption for noninvasive functional imaging,” *Phys. Rev. Appl.* **10**, 024044 (2018).
98. M. Lazebnik, L. McCartney, D. Popovic, C. B. Watkins, M. J. Lindstrom, J. Harter, S. Sewall, A. Magliocco, J. H. Booske, M. Okoniewski, S. C. Hagness, “A large-scale study of the ultrawideband microwave dielectric properties of normal breast tissue obtained from reduction surgeries,” *Phys. Med. Biol.* **52**, 2637–2656 (2007).
99. Z. X. Wang, Y. M. Zhang, B. Cao, Z. Ji, W. L. Luo, S. D. Zhai, D. D. Zhang, W. P. Wang, D. Xing, X. L. Hu, “Explosive nanocapsules excited by pulsed microwaves for efficient thermoacoustic-chemo combination therapy,” *Nanoscale* **11**, 1710–1719 (2019).
100. S. Zhai, X. Hu, Z. Ji, H. Qin, Z. Wang, Y. Hu, D. Xing, “Pulsed microwave pumped drug-free thermoacoustic therapy by high-biocompatible and safe metabolic polyarginine probes,” *Nano Lett.* **19**, 1728–1735 (2019).
101. W. Li, S. Zhang, D. Xing, H. Qin, “Pulsed microwave-induced thermoacoustic shockwave for precise glioblastoma therapy with the skin and skull intact,” *Small* **18**, 2201342 (2022).